Investigation on the cosmic-ray shadow of planets and asteroids

Yi Zhang (zhangyi@pmo.ac.cn)
Purple Mountain Observatory
Jun Li
Purple Mountain Observatory
X. Y. Huang
Purple Mountain Observatory
J. Y. He
Purple Mountain Observatory

Research Article

Keywords: Cosmic Rays, Moon Shadows, Planets, Asteroids

Posted Date: April 8th, 2022

DOI: https://doi.org/10.21203/rs.3.rs-1515432/v1

Investigation on the cosmic-ray shadow of planets and asteroids

Jun Li[1,2], Yi Zhang[1,2*], X.Y. Huang[1,2] and J.Y. He[1,2]

[1]Key Laboratory of dark Matter and Space Astronomy, Purple Mountain Observatory, Chinese Academy of Sciences, Nanjing, 210033, Jiangsu, China.
[2]School of Astronomy and Space Science, University of Science and Technology of China, Hefei, 230026, Anhui, China.

*Corresponding author(s). E-mail(s): zhangyi@pmo.ac.cn;
Contributing authors: lij@pmo.ac.cn; xyhuang@pmo.ac.cn;
hejy@pmo.ac.cn;

Abstract

The moon shadow and sun shadow of cosmic rays are commonly used to calibrate the angular resolution of the instrument in extensive air shower experiments, measure the proton-antiproton ratio, and study the interplanetary magnetic field (IMF). The shadow effect of planets and asteroids in the solar system, on the other hand, has received little attention. If considerable shadow effects can be observed, a novel approach may be developed to calibrate the point spread function and investigate the IMF. In this work, we calculate the sensitivity of observing the shadow effects of planets and asteroids in the next hundred years using LHAASO's instrumental response as an example. The result shows that the blocking impact of these celestial bodies is minimal; thus, their influence on the direction distribution of cosmic rays is negligible.

Keywords: Cosmic Rays, Moon Shadows, Planets, Asteroids

1 Introduction

Cosmic rays are blocked by some celestial objects when propagating, resulting in a shadow in the sky. We call these phenomena the shadow effect of

the celestial objects. The moon shadow[1][2] [3][4] and the sun shadow[5][6] are representatives of these phenomena. People have been studying the moon shadow and the sun shadow for a long time. As early as 1957, G.W.Clark noted the shadow effect of the moon while investigating the arrival directions of air showers.[7] Many ground-based detectors have observed moon shadow and sun shadow in the past decades, including H.E.S.S.[8], ARGO-YBJ[9], HAWC[10] and LHAASO[11].

Extensive air shower(EAS) experiments usually use the circular banded distribution of the moon shadow to determine the angular resolution[12] because the apparent radius of the moon is about 0.26°, which is small compared to the generally angular resolution of this kind of experiment. As charged cosmic rays are deflected by the geomagnetic field(GMF), the deflection angle increases with the decrease of particle's energy. Thus the EAS experiments use moon shadow to determine the detector's energy resolution [4] and study the ratio of proton and antiproton [13]. Similarly, sun shadow can be used as a calibration source for a neutrino telescope [14] and measure the interplanetary magnetic field (IMF)[15].

In addition, other celestial objects should have similar shadow effects. However, all previous research has not discussed them seriously. In this study, we analyze the shadow effects of the planets and asteroids in the solar system in this work. These sources are more like point sources, and we can use their shadow to calibrate the point spread function (PSF) of high-energy cosmic rays. It could be helpful to study IMF at lower energies. The apparent radii of these objects are relatively small, so we stack the shadow effects of these objects. With the construction and operation of modern large-scale ground-based EAS experiments, it is time to investigate the possibility of detecting the shadows of these objects.

About 120,000 asteroids have been observed; most are located in an asteroid belt between Jupiter and Mars. However, we use the data from just over 20,000 asteroids with good orbit observations due to current observation techniques. This paper will estimate the sensitivity of observing the cosmic-ray shadow effect of these objects taking LHAASOs instrumental response. Besides the analysis for individual objects, a stacked analysis is also performed.

2 Methods of analysis

We use the likelihood ratio method to estimate the significance level of the cosmic ray shadow of a celestial body. The test statistic is defined as

$$TS = 2\ln\frac{L(N_{obs}|H_1)}{L(N_{obs}|H_0)} = 2\ln\frac{Possion(N_{obs};\ N_b + N_s)}{Possion(N_{obs};\ N_b)}, \tag{1}$$

with the background-only hypothesis H_0 and the background-plus-signal hypothesis H_1. L is the likelihood; N_s is the number of blocked cosmic ray(CR) events; N_b is the background events estimated by the background estimation

method, such as the direct integral method [16] and the equi-zenith angle method [17].

In the back-ground-only case, the TS value follows a χ^2 distribution with n degrees of freedom according to the Wilks theorem [18]. For a single celestial body, the significance is S=$\sqrt{TS}$ in the case of one free parameter case. Meanwhile, as the EAS experiment will collect a large number of events, the N_b and N_{obs} follow a Gaussian distribution. The expected significance can be approximated by $S = N_s/\sqrt{N_s + N_b}$. Furthermore, N_s/N_b is small according to the moon shadow analysis due to the limited angular resolution of a EAS experiment. The significance can be expressed as

$$S = \frac{N_s}{\sqrt{N_b}}. \tag{2}$$

Both N_s and N_b depend on the zenith angle θ, they can be estimated by

$$\begin{aligned} N_s &= \int_t \pi r_o^2(t) N(t) cos^n(\theta(t)) dt \\ N_b &= \int_t \pi r_{sm}^2 N(t) cos^n(\theta(t)) dt, \end{aligned} \tag{3}$$

where r_0 is the apparent radius of a given celestial body; r_{sm} is the smooth radius; N(t) is the event rate. In general, r_0 is much less than the angular resolution of the instrument, so the smooth radius r_{sm} is mainly determined by the angular resolution. We used the same r_{sm} for planets, asteroids and moon in this work, as all these celestial bodies can be considered as point sources. The detection efficiency generally depends on the atmospheric depth the cosmic ray passes through and the effective area for collecting, thus related to the zenith angle's cosine value. We use $cos^n(\theta)$ to estimate the CR detection efficiency as a function of the zenith angle, and we obtain n = 7 from a simulation by Corsika.[19]

As the variation of N(t) is negligible, we assume that N(t) is stable. The significance now is

$$S = \frac{\sqrt{\pi N}}{r_{sm}} \frac{\int_t r_o^2(t) cos^n(\theta(t)) dt}{\sqrt{\int_t cos^n(\theta(t)) dt}}. \tag{4}$$

We define the variable $\eta = \frac{\int_t r_o^2(t) cos^n(\theta(t)) dt}{\sqrt{\int_t cos^n(\theta(t)) dt}}$ to estimate the relative significance for each celestial body.

We define $R_\eta = \eta/\eta_{moon}$, $R_{Ns} = Ns/Ns_{moon}$ to represent the significance and blocked event counts with respect to that of the moon shadow, respectively. Note that the expected significance and blocked event counts are proportional to the apparent radius square. To perform a stacked analysis, we define a stacked test statistics as [20]:

$$TS_{stack} = 2\ln\frac{L_{stack}(N_{obs}|H_1)}{L_{stack}(N_{obs}|H_0)} = 2\ln\frac{\prod_i Possion(N_{obs,i};\ N_{b,i}+N_{s,i})}{\prod_i Possion(N_{obs,i};\ N_{b,i})}. \quad (5)$$

Thus $TS_{stack} = \sum_i TS_i$. For every celestial body, we can estimate its significance with $S_i = \sqrt{TS_i}$ following the same test procedure; therefore, we obtain the expected stacked significance

$${S_{stack}}^2 = \sum_i {S_i}^2, \quad (6)$$

where S_i is significance of the ith celestial body. We end up with

$$\eta_{stack} = \sqrt{\sum_i {\eta_i}^2}, \quad (7)$$

where the η_{stack}, η_i denote stacked one and ith one, respectively.

3 Planets and asteroids

We calculated the η of every planet and η_{stack} of asteroids in the solar system. The trajectory data are set from January 1st, 2020 to December 30th, 2119, obtained from PyEphem[21]. We take the LHAASO experiment as an example and set the site at $90.52°E$, $30.11°N$[22]. The zenith angles are restricted to less than 50° because the detection efficiency and the effective area of very inclined events will worsen.

Table 1 shows the apparent radius and calculated η for the other seven planets. Jupiter and Venus, the top two planets with the largest apparent radius, are the dominant contributors. The mean apparent radius of Jupiter is 0.0053°, while that is $\sim 0.26°$ for the Moon. The apparent area ratio is 4.12×10^{-4}, while the R_η is 4.19×10^{-4}. It indicates that the effect from zenith angle distribution is minimal. We combine all the planets and obtain the stacked $R_{\eta,stack}$ of 4.6×10^{-4} using formula 7, as shown in table 2.

Till 2006, humans have discovered more than 120000 asteroids and estimate that there would be more than one million asteroids in the solar system. The asteroids studied in this paper are celestial bodies more minor than the planets we discussed in Table 1. These asteroids are distributed in the asteroid belt between Mars and Jupiter. These asteroids are approximately 2.2 to 3.6 AU away from the sun, and their revolution periods are generally 3.5 to 6 years.

All observable asteroids analysed in this paper are divided into three groups according to the standards of the Ephem database[21], which is $Critical-list\ Numbered\ Minor\ Planets$(CNMPs), $Distant\ Minor\ Planets$(DMPs) and

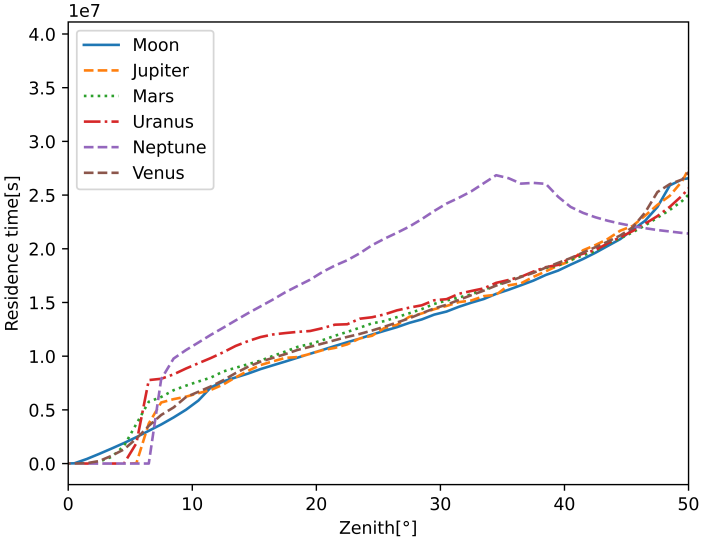

Fig. 1 The residence times of the moon and major planets at different zenith angles with from 2020 to 2119. The solid blue line indicates zenith angles' residence times for the moon, and the orange and brown dash lines are for Jupiter and Venus, respectively. Here the zenith angles are limited to less than 50°.

Table 1 The blocking effect of cosmic rays by primary planets in the solar system.

Planets	$\overline{Dis}_{sun}[AU]$	$\overline{Dis}_{earth}[AU]$	$\overline{Radius}[deg]$	$\eta[rad^2 s^{\frac{1}{2}}]$	R_η
Jupiter	5.20	5.28	5.30×10^{-3}	1.27×10^{-4}	4.19×10^{-4}
Venus	0.72	1.13	2.79×10^{-3}	5.08×10^{-5}	1.67×10^{-4}
Saturn	9.55	9.58	2.42×10^{-3}	2.67×10^{-5}	8.79×10^{-5}
Mars	1.53	1.69	9.81×10^{-4}	5.66×10^{-6}	1.87×10^{-5}
Mercury	0.39	1.04	9.76×10^{-4}	4.99×10^{-6}	1.64×10^{-5}
Uranus	19.23	19.25	5.12×10^{-4}	1.26×10^{-6}	4.19×10^{-6}
Neptune	29.99	30.02	3.16×10^{-4}	5.49×10^{-7}	1.81×10^{-6}

Note: $\overline{Dis}_{sun}$ is the average distance between the planet and the sun. $\overline{Dis}_{earth}$ is the average distance between the planet and the earth. $\overline{Radius}$ is the average apparent radius of the planet.

Unusual Minor Planets(UMPs). Figure 2 shows the apparent radii distributions of each group of asteroids. The average apparent radii for each group are listed in Table 2. The UMPs group dominates the contribution, the R_η of 5.31×10^{-5}.

4 Result and discussion

We analyse the data of 100 years of planets and asteroids in our solar system in this work. The blocked events ratio $R_{Ns,stack}$ of all celestial bodies is 1.16×10^{-3} as shown in Table 2, and combining Table 1 we can know that the UMPs

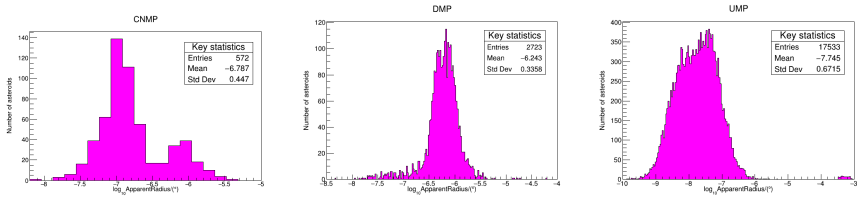

Fig. 2 The apparent radius distribution of the asteroids in the solar system(Asteroids whose apparent radii are 0° are not included.). According to [21], there are three groups of asteroids in the solar system. The three subgraphs are the apparent radius distributions of CNMPs, DMPs and UMPs, respectively.

Table 2 The shadow effects on cosmic rays of asteroids.

Asteroids	*Number*	$\overline{Radius}[deg]$	$R_{Ns_{stack}}$	$\eta_{stack}[rad^2 s^{\frac{1}{2}}]$	$R_{\eta_{stack}}$
CNMPs	650	3.05×10^{-7}	3.54×10^{-9}	1.31×10^{-10}	4.32×10^{-10}
DMPs	3747	7.55×10^{-7}	4.29×10^{-7}	8.23×10^{-8}	2.71×10^{-7}
UMPs	18169	2.23×10^{-6}	4.40×10^{-4}	1.61×10^{-5}	5.31×10^{-5}
Planets	7	-	7.20×10^{-4}	1.39×10^{-4}	4.60×10^{-4}
All	22573	-	1.16×10^{-3}	1.40×10^{-4}	4.61×10^{-4}

and Jupiter make up the majority. The time evolution of η over 100 years is shown in Figure 3. The red solid line indicates the stacked η for all planets and

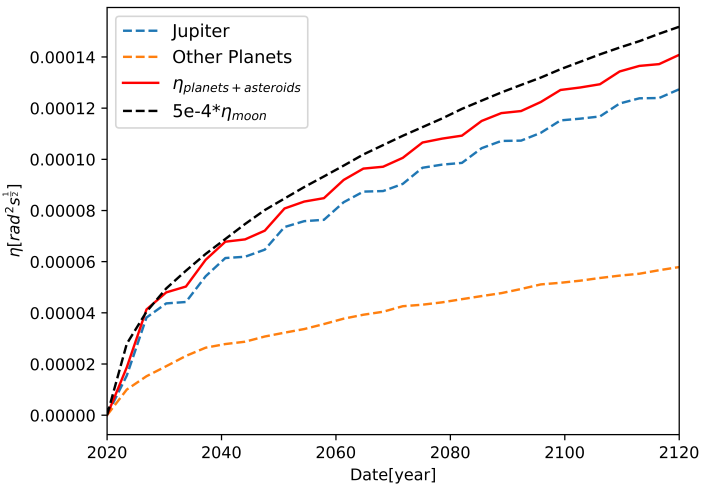

Fig. 3 Change in η over time of the moon and major planets from 2020 to 2119. Here the zenith angles are limited to less than 50.

asteroids in 100 years. The black dash line is the $5 \times 10^{-4}\eta_{moon}$. The stacked value of R_η is about 4.61×10^{-4} for all the planets and asteroids. If we want to observe these shadow effects with the significance of 5σ, the significance value

of the moon shadow needs to reach 10846σ. Each month, the significance value of moon shadow is estimated as 25σ at $\sim$20 TeV for LHAASO-KM2A[23][24] and 30σ at $\sim$ 1 TeV for LHAASO-WCDA [25], respectively. To get a shadow effect with 5σ, it will take 15685 years for KM2A and 10892 years for WCDA.

The blocking effect of these celestial bodies is mainly related to the square of their apparent radii. The stacked blocking area is much less than that of the moon, so the influence on the direction of cosmic rays caused by these celestial bodies' shadow effect is negligible.

The total five σ significance of all these objects is expected to be observed by LHAASO in a very long time. However, future experiments will give actual observations with the continuous improvement of observation technology, e.g., improved angular resolution and effective area. If the PSF is much less than the moons apparent radius, the cosmic ray shadow of planets and asteroids discussed in this work can be served as point sources to calibrate the angular resolution for high-energy cosmic rays.

Furthermore, studying the planets' shadows could play an essential role in analyzing GMF and IMF. The relationship between IMF and heliocentric distance is given in [26]. Previously, the relationship between IMF and heliocentric distance based on the variation of sun shadow has been analyzed.[26] If the planets' shadows are significant enough, we can use them to test models about IMF. The planets' shadow effect provides a variety of methodological choices for the analysis of GMF and IMF because the distances between the planets and the Earth are diverse (ranging from 1.04AU to 30.02AU, as shown in Table 1).

Declarations

- **Funding**
  This work is supported in China by the National Key R&D program of China under the grants 2018YFA0404202, by the National Natural Science Foundation of China under the grants 11775233 and the Program for Innovative Talents and Entrepreneur in Jiangsu.
- **Competing interests**
  The authors declare no competing interests.
- **Ethics approval**
  Not applicable.
- **Consent to participate**
  Not applicable.

- **Availability of data and materials**
  Correspondence and requests for materials should be addressed to Yi Zhang (zhangyi@pmo.ac.cn) or Jun Li (lij@pmo.ac.cn).

- **Authors' contributions**

Yi Zhang raises the project, guiding the data analysis, paper writing, and revision. Jun Li is the executor of the experimental research, completing data analysis and writing the first draft of the paper. J.Y. He participates in method design, result verification, and paper revision. X.Y. Huang engages in the writing and revision of the article. All authors read and agree on the final text.

References

[1] Aartsen, M., Abbasi, R., Abdou, Y., Ackermann, M., Adams, J., Aguilar, J., Ahlers, M., Altmann, D., Auffenberg, J., Bai, X., *et al.*: Observation of the cosmic-ray shadow of the moon with icecube. Physical Review D **89**(10), 102004 (2014)

[2] Abeysekara, A., Albert, A., Alfaro, R., Alvarez, C., Álvarez, J., Arceo, R., Arteaga-Velázquez, J., Rojas, D.A., Solares, H.A., Belmont-Moreno, E., *et al.*: Constraining the p^-/p ratio in tev cosmic rays with observations of the moon shadow by hawc. Physical Review D **97**(10), 102005 (2018)

[3] Colin, P., Tridon, D.B., Ortega, A.D., Doert, M., Doro, M., Pochon, J., Strah, N., Suric, T., Teshima, M.: Probing the cr positron/electron ratio at few hundreds gev through moon shadow observation with the magic telescopes. arXiv preprint arXiv:1110.0183 (2011)

[4] Wang, Y., Cao, Z., Zeng, Z., Mab, L., et al.: The energy scale calibration using the moon shadow of lhaaso-wcda detector. 37th ICRC (2021) (2021)

[5] Amenomori, M., Bi, X., Chen, D., Chen, T., Chen, W., Cui, S., Ding, L., Feng, C., Feng, Z., Feng, Z., *et al.*: Probe of the solar magnetic field using the cosmic-ray shadow of the sun. Physical review letters **111**(1), 011101 (2013)

[6] Tjus, J.B., Desiati, P., Döpper, N., Fichtner, H., Kleimann, J., Kroll, M., Tenholt, F.: Cosmic-ray propagation around the sun: investigating the influence of the solar magnetic field on the cosmic-ray sun shadow. Astronomy & Astrophysics **633**, 83 (2020)

[7] Clark, G.W.: Arrival directions of cosmic-ray air showers from the northern sky. Physical Review **108**(2), 450 (1957)

[8] Hofmann, W., collaboration, H., *et al.*: Status of the hess project. In: International Cosmic Ray Conference, vol. 5, p. 2811 (2003)

[9] Cao, Z.: The argo-ybj experiment progresses and future extension. International Journal of Modern Physics D **20**(10), 1713–1721 (2011)

[10] Smith, A.J.: Hawc: Design, operation, reconstruction and analysis. arXiv preprint arXiv:1508.05826 (2015)

[11] Di Sciascio, G., Collaboration, L., *et al.*: The lhaaso experiment: from gamma-ray astronomy to cosmic rays. Nuclear and particle physics proceedings **279**, 166–173 (2016)

[12] Bartoli, B., Bernardini, P., Bi, X., Bleve, C., Bolognino, I., Branchini, P., Budano, A., Melcarne, A.C., Camarri, P., Cao, Z., *et al.*: Observation of the cosmic ray moon shadowing effect with the argo-ybj experiment. Physical Review D **84**(2), 022003 (2011)

[13] Grabski, V., Morales, A., Reche, R., Orozco, O.: Feasibility for p+/p-flow-ratio evaluation in the 0.5-1.5 tev primary energy range, based on moon-shadow muon measurements, to be carried out in the pyramid of the sun, teotihuacan, experiment. arXiv preprint arXiv:0705.4332 (2007)

[14] Albert, A., André, M., Anghinolfi, M., Anton, G., Ardid, M., Aubert, J.-J., Aublin, J., Baret, B., Basa, S., Belhorma, B., *et al.*: Observation of the cosmic ray shadow of the sun with the antares neutrino telescope. Physical Review D **102**(12), 122007 (2020)

[15] Aielli, G., Bacci, C., Bartoli, B., Bernardini, P., Bi, X., Bleve, C., Bolognino, I., Branchini, P., Budano, A., Bussino, S., *et al.*: Mean interplanetary magnetic field measurement using the argo-ybj experiment. The Astrophysical Journal **729**(2), 113 (2011)

[16] Ackermann, M., Ajello, M., Atwood, W., Baldini, L., Ballet, J., Barbiellini, G., Bastieri, D., Bechtol, K., Bellazzini, R., Berenji, B., *et al.*: Searches for cosmic-ray electron anisotropies with the fermi large area telescope. Physical Review D **82**(9), 092003 (2010)

[17] Amenomori, M.: A northern sky survey for tev gamma-ray sources using the tibet-iii air shower array (2005)

[18] Wilks, S.S.: The Large-Sample Distribution of the Likelihood Ratio for Testing Composite Hypotheses. Annals of Mathematical Statistics **9**(1), 60–62 (1938). https://doi.org/10.1214/aoms/1177732360

[19] Heck, D., Knapp, J., Capdevielle, J., Schatz, G., Thouw, T., et al.: Corsika: A monte carlo code to simulate extensive air showers. Report fzka **6019**(11) (1998)

[20] He, D.-Z., Bi, X.-J., Lin, S.-J., Yin, P.-F., Zhang, X.: Expected lhaaso sensitivity to decaying dark matter signatures from dwarf galaxies gamma-ray emission. Chinese Physics C **44**(8), 085001 (2020)

[21] Rhodes, B.C.: Pyephem: astronomical ephemeris for python. Astrophysics Source Code Library, 1112 (2011)

[22] Jiang, K., Tang, Z., Li, X., Cao, Z., Wu, X.: Qualification tests of 997 8-inch photomultiplier tubes for the water cherenkov detector array of the lhaaso experiment. Nuclear Instruments and Methods in Physics Research Section A Accelerators Spectrometers Detectors and Associated Equipment (10), 165108 (2021)

[23] Nan, Y., Li, Z., Chen, S., Feng, C., Wu, S., Li, Y.: The performances of the LHAASO-KM2A tested by the observation of cosmic-ray Moon shadow. In: Proceedings of 37th International Cosmic Ray Conference — PoS(ICRC2021), vol. 395, p. 350 (2021). https://doi.org/10.22323/1.395.0350

[24] Huang, Z., Huang, D., Zhou, X., Zhao, J., He, H., Chen, S., Ma, X., Liu, D., Axi, K., et al.: Simulation study on scaler mode in lhaaso-km2a (2021)

[25] Wang, Y., Cao, Z., Zeng, Z., Ma, L., Nan, Y.: The Energy Scale Calibration using the Moon Shadow of LHAASO-WCDA Detector. In: Proceedings of 37th International Cosmic Ray Conference — PoS(ICRC2021), vol. 395, p. 356 (2021). https://doi.org/10.22323/1.395.0356

[26] Behannon, K.W.: Heliocentric distance dependence of the interplanetary magnetic field. Reviews of Geophysics **16**(1), 125–145 (1978)